Macedonian Journal of Chemistry and Chemical Engineering, Vol. **45**, No. 1, pp. xx–xx (2026)

MJCCA9 –

ISSN 1857-5552
e-ISSN 1857-5625

Received: February 3, 2026
Accepted: March 23, 2026

DOI: 10.20450/mjcce.2026.3446
Original scientific paper

DISCRIMINANT ANALYSIS OF ATORVASTATIN CALCIUM TRIHYDRATE RAW MATERIALS FROM DIFFERENT PROVIDERS BY RAMAN SPECTROSCOPY AND X-RAY DIFFRACTION IN CONJUNCTION WITH TWO-TRACE TWO-DIMENSIONAL CORRELATION

Dragana Trajkovikj Terziski[1,2], Biljana Pejova[1], Gjorgji Petrushevski[2], Ljupcho Pejov[1*]

[1]*Institute of Chemistry, Faculty of Natural Sciences and Mathematics, Ss Cyril and Methodius University, Skopje, Republic of North Macedonia*
[2]*Quality Control Pharmaceuticals, Alkaloid AD – Skopje, Aleksandar Makedonski 12, 1000 Skopje, Republic of North Macedonia*
ljupcop@pmf.ukim.mk

Two-trace two-dimensional (2T2D) correlation of Raman spectroscopy and X-ray diffraction data was applied for discriminant analysis of atorvastatin calcium trihydrate raw material samples from two different manufacturers. Single-parameter trace similarity measures, such as cosine distance and Pearson's correlation coefficient, often fail to properly reflect the differences between complex two-dimensional traces containing numerous signals. The discriminant potential of asynchronous 2T2D correlation maps constructed from Raman spectra and X-ray diffraction patterns (XRD) proved exceptional for resolving overlapping bands from multiple species and revealing complementary phase composition information in raw material samples (including active pharmaceutical ingredients – APIs). Under stringent regulatory demands for quality assurance, batch uniformity, and trace impurity detection, this method provides a practical, complementary QC routine that enables rapid polymorph identification. This study demonstrates the application of 2T2D correlation analysis integrated with Raman spectroscopy and XRD as a feasible, complementary method for quality control and assurance of APIs.

Keywords: atorvastatin calcium trihydrate; Raman spectroscopy; X-ray diffraction; two-trace two-dimensional correlation spectroscopy

ДИСКРИМИНАНТНА АНАЛИЗА НА СУРОВИНИ ОД АТОРВАСТАТИН КАЛЦИУМ ТРИХИДРАТ ОД РАЗЛИЧНИ ДОБАВУВАЧИ СО РАМАНСКА СПЕКТРОСКОПИЈА И ДИФРАКЦИЈА НА РЕНДГЕНСКИ ЗРАЦИ ВО СПРЕГА СО ДВОКАНАЛНА ДВОДИМЕНЗИОНАЛНА КОРЕЛАЦИОНА АНАЛИЗА

Применета е двоканална дводимензионална (2T2D) корелациона анализа на податоци добиени со Раманска спектроскопија и дифракција на рендгенски зраци за дискриминантна анализа на суровини од аторвастатин калциум трихидрат од два различни добавувачи. Еднопараметарските мерки за сличност на информационите канали, како што се косинусното растојание и Пирсоновиот коефициент на корелација, најчесто не успеваат соодветно да ги рефлектираат разликите помеѓу комплексни дводимензионални канали кои содржат голем број на сигнали. Дискриминантниот потенцијал на асинхроните 2T2D корелациони мапи конструирани од Раманските спектри и дифрактограмите се покажа како исклучителен за разграничување на преклопени ленти од повеќе различни видови како и за откривање на комплементарни информации за фазниот состав на примероци од суровини (вклучувајќи фармацевтски активни состојки – API). Во услови на строги регулаторни барања за обезбедување на квалитет, униформност на серии и детекција на траги од онечистувања, овој метод претставува практична, комплементарна постапка за контрола на квалитет (QC) која што овозможува брза идентификација

на полиморфи. Оваа студија ја демонстрира примената на 2T2D корелационата анализа интегрирана со Раманска спектроскопија и дифракција на рендгенски зраци како изводлив и комплементарен метод за контрола и обезбедување на квалитетот на фармацевтски активните состојки.

Клучни зборови: аторвастатин калциум трихидрат; Раманска спектроскопија; дифракција на рендгенски зраци; двоканална дводимензионална корелациона спектроскопија

1. INTRODUCTION

Atorvastatin calcium (Atorvastatin Ca), with the systematic chemical name, (3R,5R)-7-[2-(4-fluorophenyl)-3-phenyl-4-(phenylcarbamoyl)-5-(propan-2-yl)-1H-pyrrol-1-yl]-3,5-dihydroxyheptanoic acid calcium salt is a widely prescribed lipid-lowering agent characterized by low solubility and high permeability. Originally approved by The Food and Drug Administration (FDA) (1996), its API and tablet formulations are governed by United States Pharmacopeia (USP) specifications due to intense regulatory scrutiny from agencies such as the FDA, European Medicines Agency (EMA), and other pharmacopeias concerning batch consistency, trace impurities, and degradation products from salt disproportionation. Since its market introduction, atorvastatin has played a central role in the management of dyslipidemia and the primary and secondary prevention of cardiovascular events. Its mechanism of action involves the reversible inhibition of 3-hydroxy-3-methylglutaryl-coenzyme A (HMG-CoA) reductase, a key enzyme in the mevalonate pathway of cholesterol biosynthesis. By lowering hepatic cholesterol production, atorvastatin reduces plasma levels of total cholesterol, low-density lipoprotein (LDL) cholesterol (LDL-C), and triglycerides, while increasing high-density lipoprotein (HDL) cholesterol (HDL-C) to a lesser extent.[1–3] Beyond lipid modification, atorvastatin has demonstrated pleiotropic effects, including improvements in endothelial function, anti-inflammatory benefits, and stabilization of atherosclerotic plaques, making it a critical therapy in both cardiology and internal medicine.[4–8] Atorvastatin's prominence is further underscored by its inclusion in various national and international treatment guidelines for hyperlipidemia. Its formulations, as both monotherapy and in combination with other agents, such as amlodipine, are registered as essential medicines by the World Health Organization (WHO).

Atorvastatin calcium exhibits polymorphism and pseudopolymorphism (e.g., the trihydrate form), with multiple forms impacting kinetic and thermodynamic stability, processability, and detectability thresholds. During Phase III clinical trials, the crystalline Form I was identified as a trihydrate. This form exhibited remarkable solid-state properties, offering superior processability compared with the amorphous form, and an enhanced stability of tablet formulations. Although differences were observed in absorption rate, the extent of absorption was proven to be equivalent in bioequivalence studies. Additional patented forms include Forms II, IV, and V.

This polymorphic diversity underscores the importance of characterizing and monitoring the solid-state forms during development, manufacturing, and storage.[8–12] As with many complex active pharmaceutical ingredients (APIs), ensuring the consistent quality of atorvastatin calcium requires sensitive and specific analytical techniques capable of distinguishing between the API, its impurities, and degradation products, often present at trace levels or in minute quantities. Such phase versatility in multicomponent solids demands analytical techniques capable of distinguishing even trace amounts of different forms.

High-performance liquid chromatography (HPLC) is the gold standard for quantifying and assessing the purity of atorvastatin calcium, often coupled with ultraviolet-visible (UV–Vis) spectroscopy or mass spectrometry for enhanced sensitivity and impurity profiling.[10] Thin-layer chromatography (TLC) and high-performance TLC (HPTLC) are employed for rapid screening and impurity checks, especially if advanced instrumentation is unavailable.[10,11] UV–Vis spectrophotometry provides a simple, low-cost method for content uniformity assessment but suffers from limited selectivity. Liquid chromatography–mass spectrometry (LC–MS) and gas chromatography–mass spectrometry (GC–MS) are essential for the precise identification of impurities and metabolites. Fourier transform infrared (FTIR) spectroscopy is useful for rapid, non-destructive structural analysis and excipient compatibility testing. While each technique offers specific advantages, they also possess inherent limitations.[12]

Despite their robustness, as noted previously, conventional chromatographic and spectroscopic methods face significant challenges, especially

when resolving highly overlapping spectra or when subtle changes in molecular structure induce only minor spectral shifts. Trace impurities or subtle physical changes arising from polymorphic transitions may lie below the detection limit or remain masked within traditional one-dimensional (1D) spectra.[10–12] These limitations have driven the adoption of more sophisticated, multidimensional techniques in pharmaceutical research.

In the present study, we employed Raman spectroscopy and X-ray diffraction techniques, in conjunction with two-trace two-dimensional correlation analysis, to perform discriminant analysis of atorvastatin calcium trihydrate raw material samples from two different commercially available manufacturers.

2. EXPERIMENTAL

Atorvastatin calcium samples were obtained from Alkaloid AD, Skopje, North Macedonia, which sourced them from two different commercially available manufacturers (denoted as Producer 1 and Producer 2 throughout the manuscript). By convention, the sample provided by Producer 1 was designated as the generic "test" sample, while the one provided by Producer 2 was designated as the "reference".

2.1. *Raman spectroscopy and X-ray diffraction*

Raman spectra of atorvastatin calcium were acquired using a NanoRam-1064 spectrometer (Metrohm Group, USA) operating in Investigation mode, utilizing a point-and-shoot adapter for non-destructive measurement of the sample bags containing the powder, directly in the quality control (QC) warehouse. Measurements were performed using the default Operation Preset (min hit quality index (HQI) = 93; Raman shift range: 176–2500 cm^{-1}), with spectra collected from multiple spots in order to facilitate subsequent two-trace two-dimensional (2T2D) correlation analysis. X-ray diffraction (XRD) patterns were recorded on an Ultima IV X-ray diffractometer (Rigaku Co., Japan) using CuK_α radiation, operating in the θ–2θ scanning mode with a step-scan size of $\Delta(2\theta)$ = 0.02 °.

3. RESULTS AND DISCUSSION

3.1. *Trace similarity measures*

The simplest procedure employed to obtain a quantitative assessment of the similarity between two spectral traces involved the vector representation of the spectra and the subsequent computation of the cosine similarity score. The two relevant spectral traces *x* and *y*, were treated as vectors in *n*-dimensional space (R^n):

$$\vec{x} = [x_1, x_2, \ldots x_n] \quad (1)$$

$$\vec{y} = [y_1, y_2, \ldots y_n] \quad (2)$$

The scalar (dot) product of these two vectors was defined as:

$$(\vec{x} \cdot \vec{y}) = |\vec{x}| \cdot |\vec{y}| \cdot \cos\theta \quad (3)$$

which, in coordinate representation, takes the form:

$$(\vec{x} \cdot \vec{y}) = \sum_{i=1}^{n} x_i y_i \quad (4)$$

The norm of each of the vectors in coordinate representation was calculated as:

$$|\vec{x}| = \sqrt{\sum_{i=1}^{n} x_i^2} \quad (5)$$

$$|\vec{y}| = \sqrt{\sum_{i=1}^{n} y_i^2} \quad (6)$$

The cosine score, often termed the cosine similarity between the two vectors, was then defined as:[13,14]

$$cos\theta = \frac{\sum_{i=1}^{n} x_i y_i}{\sqrt{\sum_{i=1}^{n} x_i^2} \cdot \sqrt{\sum_{i=1}^{n} y_i^2}} \quad (7)$$

The parameter defined in Equation (7) is often referred to as the simple match score, or the cosine of the spectral contrast angle. Mathematically, it served as a measure of the spectral overlap, derived from the Cauchy–Schwarz inequality in *n*-dimensional Euclidean space R^n, representing the angle between the vectors $\vec{x}$ and $\vec{y}$ in R^n.

A complementary measure to the match score was Pearson's correlation coefficient.[15] This quantity was defined as:

$$r_{\text{Pearson}} = \frac{\sum_{i=1}^{n} (x_i - \bar{x}) \cdot (y_i - \bar{y})}{\sqrt{\sum_{i=1}^{n} (x_i - \bar{x})^2} \cdot \sqrt{\sum_{i=1}^{n} (y_i - \bar{y})^2}} \quad (8)$$

In Equation (8), $\bar{x}$ and $\bar{y}$ represented the corresponding mean values. In the present study, we calculated the cosine distances and the Pearson's correlation coefficient between the Raman spectra and the X-ray diffraction patterns of atorvastatin calcium trihydrate from the two different manufacturers. The results are summarized in Table 1.

T a b l e 1

Calculated cosine distance scores and Pearson's correlation coefficients between the Raman spectra and the powder XRD patterns for the two atorvastatin calcium trihydrate samples obtained from two different manufacturers (see text for details)

	XRD	Raman
Cosine similarity	0.9599	0.9992
Pearson's correlation	0.9181	0.9989

The calculated cosine scores and the Pearson's correlation coefficients revealed high similarity between the Raman spectra of the atorvastatin calcium trihydrate specimens from the two different manufacturers, and somewhat lower, though still substantial, similarity between the powder XRD patterns. While such single-parameter characteristics are useful when analyzing a set containing more than two samples, a single number often fails to capture the differences (or lack thereof) between complex two-dimensional traces that contain a wide variety of signals. We therefore employed two-trace two-dimensional (2T2D) correlation analysis on both the spectroscopic and diffraction data to gain further insight into the subtle differences between the studied atorvastatin samples.

3.2. *Two-trace two-dimensional (2T2D) correlation analysis*

The 2T2D method can be considered as a special case of the generalized two-dimensional correlation spectroscopic approach (GEN-2DCOS) in which only two spectral traces are compared and analyzed.[16–23] In this study, the two analyzed traces comprised pairs of Raman spectra and pairs of the powder XRD patterns obtained from atorvastatin calcium trihydrate samples derived from the two different manufacturers. One of the two traces was, by convention, designated as the "sample", while the other was designated as the "reference". The synchronous 2T2D spectrum was defined in this study as:[8,17]

$$\Phi(\nu_1,\nu_2) = \frac{1}{2}[s(\nu_1)\cdot s(\nu_2) + r(\nu_1)\cdot r(\nu_2)] \quad (9)$$

In an analogous manner, the asynchronous spectrum was defined as:

$$\Psi(\nu_1,\nu_2) = \frac{1}{2}[s(\nu_1)\cdot r(\nu_2) - r(\nu_1)\cdot s(\nu_2)] \quad (10)$$

In the previous equations, the independent variable ν represented either the Raman shift (expressed on the wavenumber scale) or the 2θ value expressed in degrees for X-ray diffraction data.

As a preliminary step prior to 2T2D analysis, the simple difference spectra were defined as:[16]

$$d(\nu) = s(\nu) - r(\nu) \quad (11)$$

By convention, the sample provided by Producer 1 was designated as the "sample" trace, while the one provided by Producer 2 was designated as the "reference" trace. Figures 1 and 2 display the computed difference spectra for pairs of Raman and XRD traces. In both cases, these spectra were bisignate. Since the Raman spectra and XRD patterns of both samples were acquired with the same instrument under identical conditions at sequential time points, the observed property of $d(\nu)$ provided a strong indication that the spectral contribution of one of the components was more prominent in the sample than in the reference spectrum.[16,17]

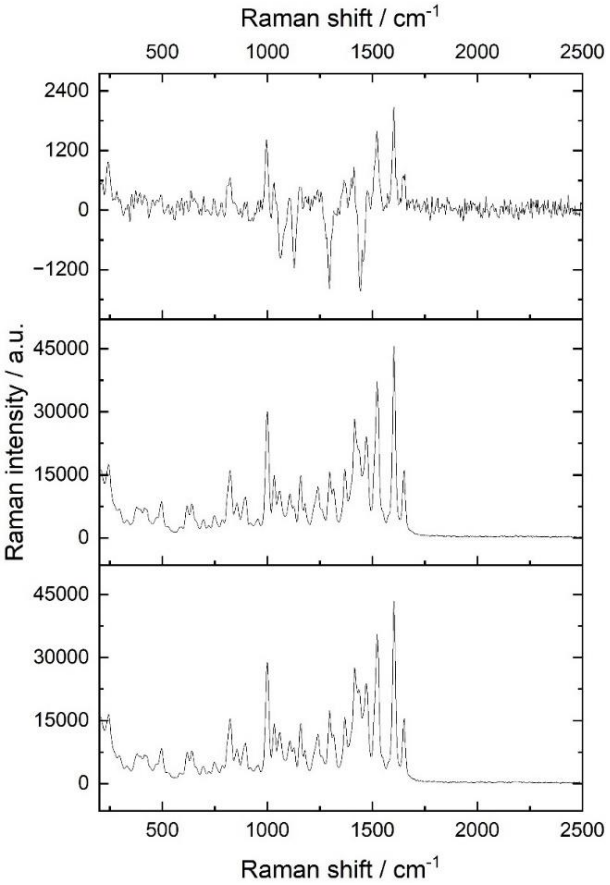

Fig. 1. The computed difference Raman spectrum (the uppermost curve) along with the respective pair of $s(\nu)$ and $r(\nu)$ traces displayed below in that order (see text for details)

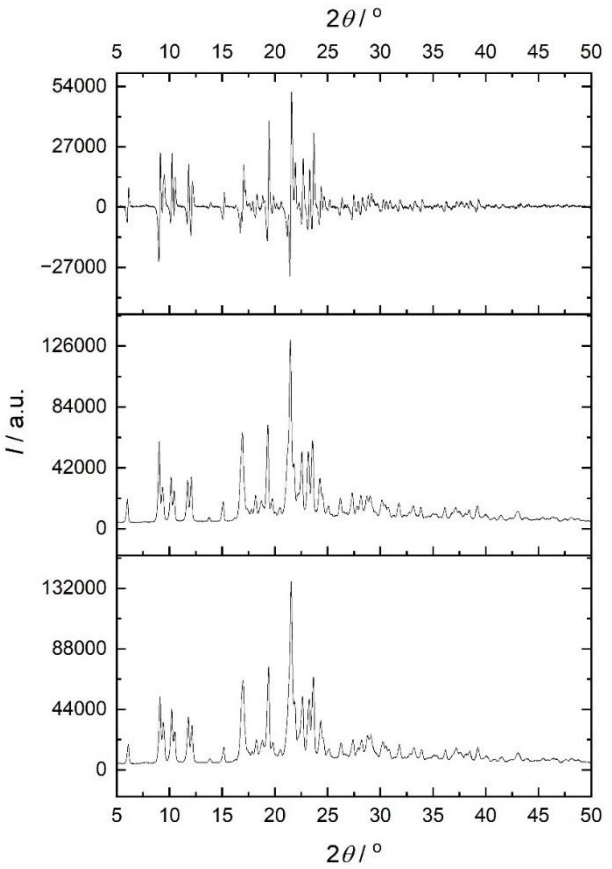

Fig. 2. The computed difference X-ray diffraction pattern (the uppermost curve) along with the respective pair of *s*(*v*) and *r*(*v*) traces displayed below in that order (see text for details).

Figures 3 and 4 display the asynchronous 2T2D spectra that were computed from the Raman spectral traces and from the powder XRD patterns. The interpretation of 2T2D correlation spectra in the present study was rationalized with the aid of a phase-space representation. To facilitate such interpretation, we employed the complex dynamic spectrum:[16,17,20]

$$a(v) = r(v) + i \cdot s(v) \qquad (12)$$

where i denotes the imaginary unit ($i = \sqrt{-1}$). Within this phase-space representation, the 2T2D correlation spectrum was reduced to a vector product of the form:

$$a(v) \cdot a^*(v) = \Phi(\nu_1, \nu_2) + i \cdot \Psi(\nu_1, \nu_2) \qquad (13)$$

Being a vector product, the complex dynamic spectrum (13) was treated as a vector in the complex Gauss plane, with a real component *r*(*v*) and an imaginary component *s*(*v*). By defining a phase angle $\Theta(\nu_1, \nu_2)$:

$$\Theta(\nu_1, \nu_2) = \arctan\left[\frac{\Psi(\nu_1, \nu_2)}{\Phi(\nu_1, \nu_2)}\right] \qquad (14)$$

we employed 2T2D analysis to compare the phase angles of two vectors in the complex plane, corresponding to the studied pairs of spectra. For the purpose of the present study, useful information was contained in the asynchronous 2T2D spectra; consequently, our focus was directed toward their analysis.

The basic physical principle underlying the 2T2D correlation analysis scheme was based on the rationale that intensity variations of bands originating from the same species in a mixture were synchronized.[16,17,20] If different bands, measured at different values of the spectral independent variables, originated from the same source, they could not change independently. Therefore, the intensity ratios were invariant. It followed from these arguments that the existence of a cross-peak in the asynchronous 2T2D spectrum implied that the bands appearing at the spectral coordinates of the cross-peak were of different origin (i.e., were due to different sources). Signals of different origin could contribute independently to the spectral traces *s*(*v*) and *r*(*v*). Analogously, the non-existence of a cross-peak at a given spectral coordinate (v_1, v_2) in the asynchronous 2T2D spectrum strongly implied that the two bands (corresponding to the specified coordinates) were of the same origin (i.e., derived from the same source). Furthermore, the positive sign of a cross-peak at (v_1, v_2), i.e., $\Psi(v_1, v_2) > 0$, implied that the contribution of the species giving rise to the signal at v_1 was dominantly represented in *s*(*v*) relative to *r*(*v*). An opposite conclusion held in the case where $\Psi(v_1, v_2) < 0$.

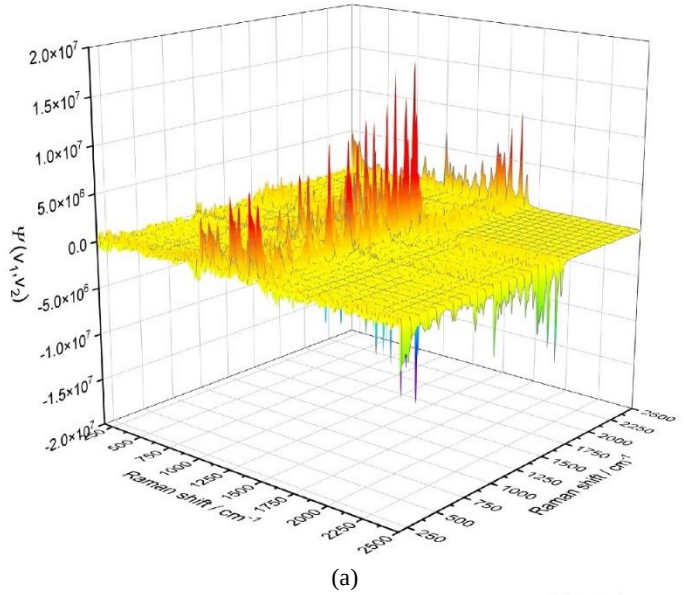

(a)

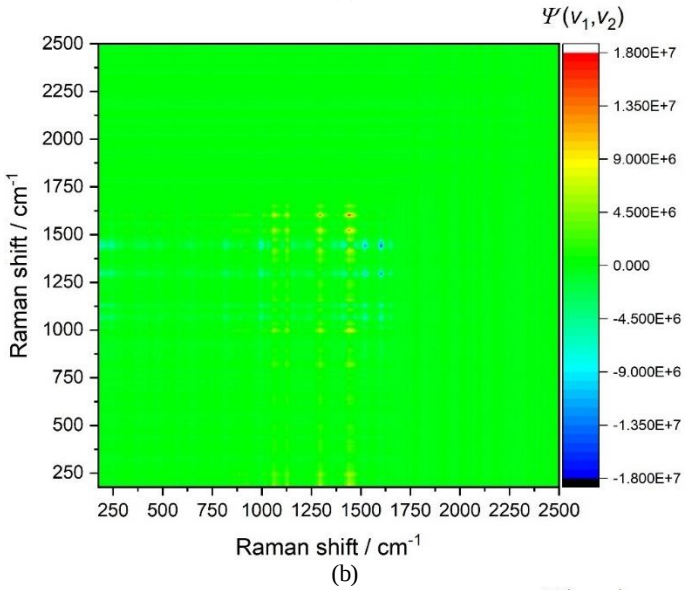

(b)

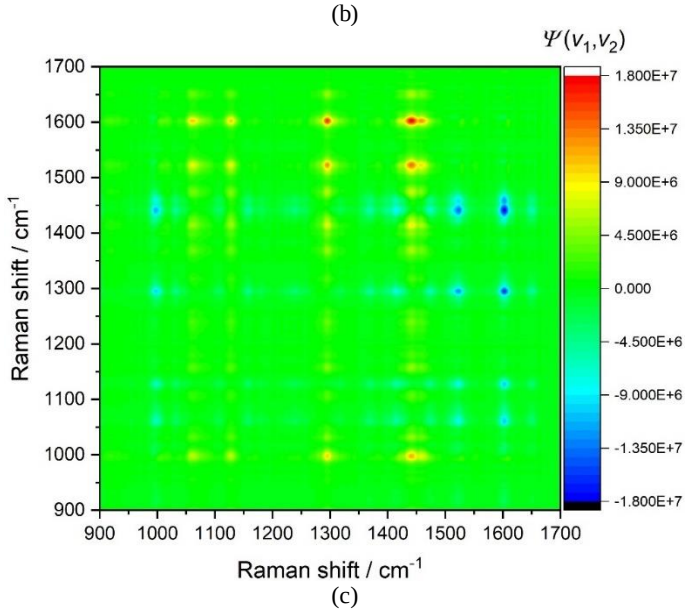

(c)

Fig. 3. Asynchronous 2T2D spectra computed from the Raman spectral traces of two atorvastatin calcium trihydrate samples: (a) a full 3D representation; (b) and (c), two-dimensional contour plots in different spectral regions (where (c) is a magnified segment of (b)

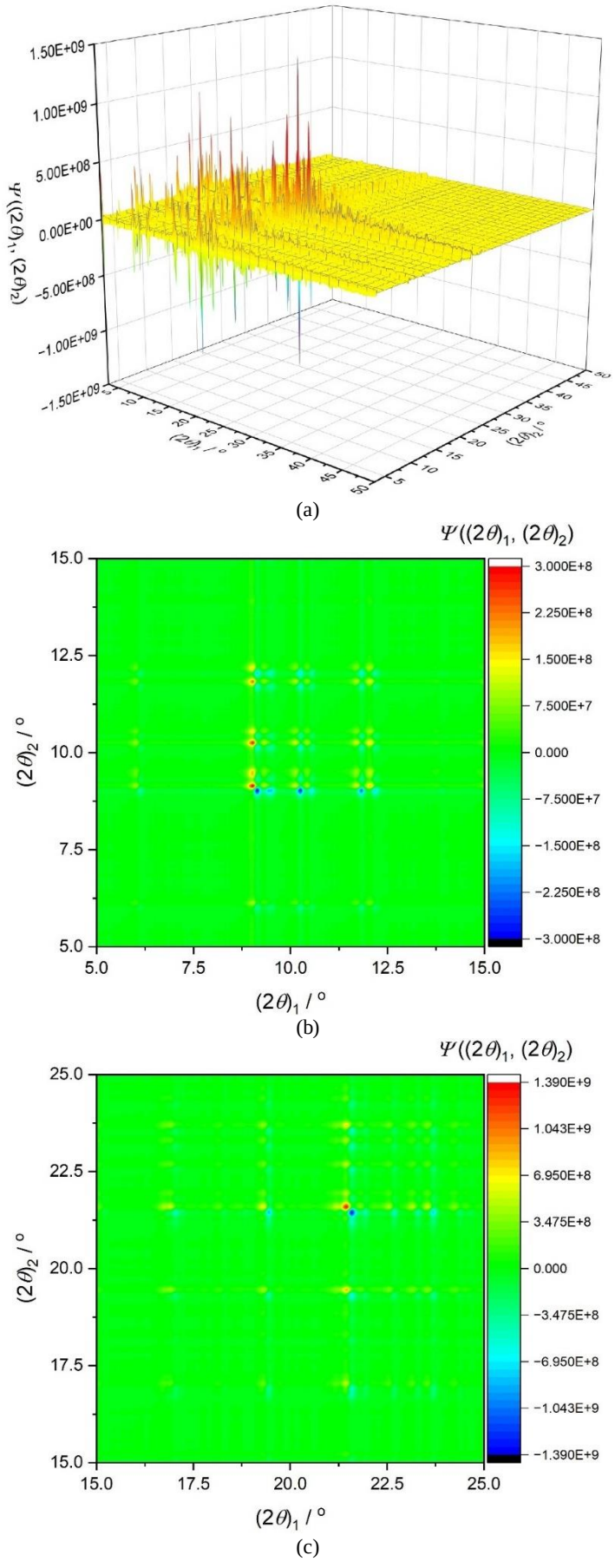

Fig. 4. Asynchronous 2T2D spectra computed from the powder X-ray diffraction traces of two atorvastatin calcium trihydrate samples: (a) full 3D representation; (b), (c), two-dimensional contour plots in different spectral regions

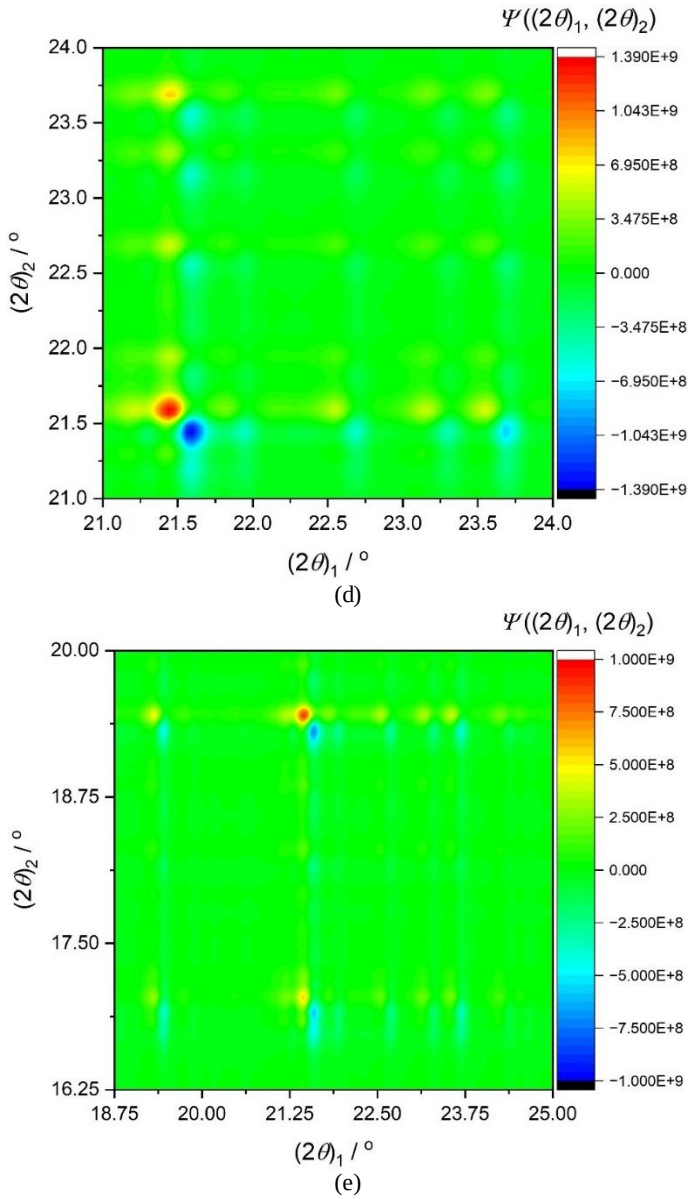

Fig. 4. Asynchronous 2T2D spectra computed from the powder X-ray diffraction traces of two atorvastatin calcium trihydrate samples: (d), two-dimensional contour plots in different spectral regions; (e) a magnified view of a segment containing the most prominent cross-peaks (see text for details)

As evident from Figures 3 and 4, the discriminating power of the asynchronous 2T2D correlation spectra was exceptional for resolving spectral bands originating from multiple species. Concurrently, the resolution of highly overlapped peaks in the 1D Raman spectrum was markedly enhanced in the 2T2D correlation map. As an example, Figures 5 and 6 present slices through the full 2T2D correlation Raman spectra at ν_1 = 1600 cm^{-1} and 1444 cm^{-1}. In Figure 5, a series of prominent negative intensity peaks ($\Psi(\nu_1, \nu_2) < 0$) are observed at the spectral coordinate ν_2 = 1060, 1128, 1296, 1440, and 1460 cm^{-1}. Figure 6, by contrast, displays a series of positive intensity peaks ($\Psi(\nu_1, \nu_2) > 0$) at the spectral coordinate ν_2 = 824, 996, and 1416 cm^{-1}. These findings indicated a different origin for the Raman band at 1600 cm^{-1} compared with those at 1060, 1128, 1296, 1440, and 1460 cm^{-1}, with the 1600 cm^{-1} band being dominantly represented in $r(\nu)$. Conversely, the band at 1444 cm^{-1} was determined to have a different origin from those at 824, 996, and 1416 cm^{-1} and was dominantly represented in $s(\nu)$. Analogous analyses were performed for all other 2T2D correlation peaks appearing in the contour map presented in Figure 3c. Due to the complexity of atorvastatin phase behavior and its degradation pathways, unambiguous assignment of all bands visible in the

2T2D correlation maps was not possible.[24-26] However, based on the literature assignments and the arguments outlined in the subsequent paragraph, we concluded that the sequence of signals appearing in the slices through the full 2T2D correlation Raman spectra at ν_1 = 1600 cm^{-1} and 1444 cm^{-1} was attributable to polymorph X of the studied compound.

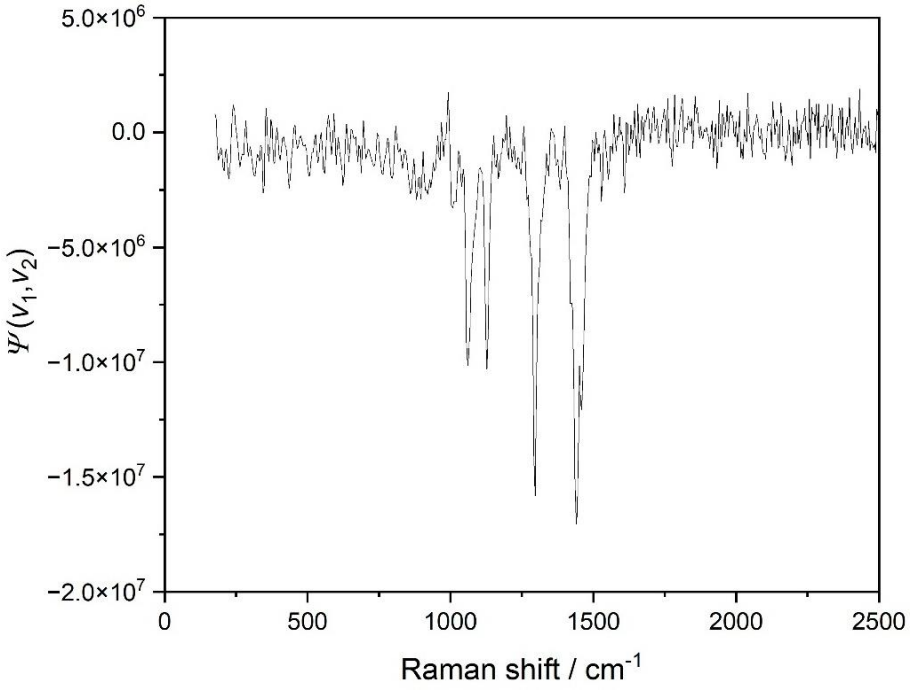

Fig. 5. Slice through the full 2T2D correlation Raman spectra at ν_1 = 1600 cm^{-1} (see text for details)

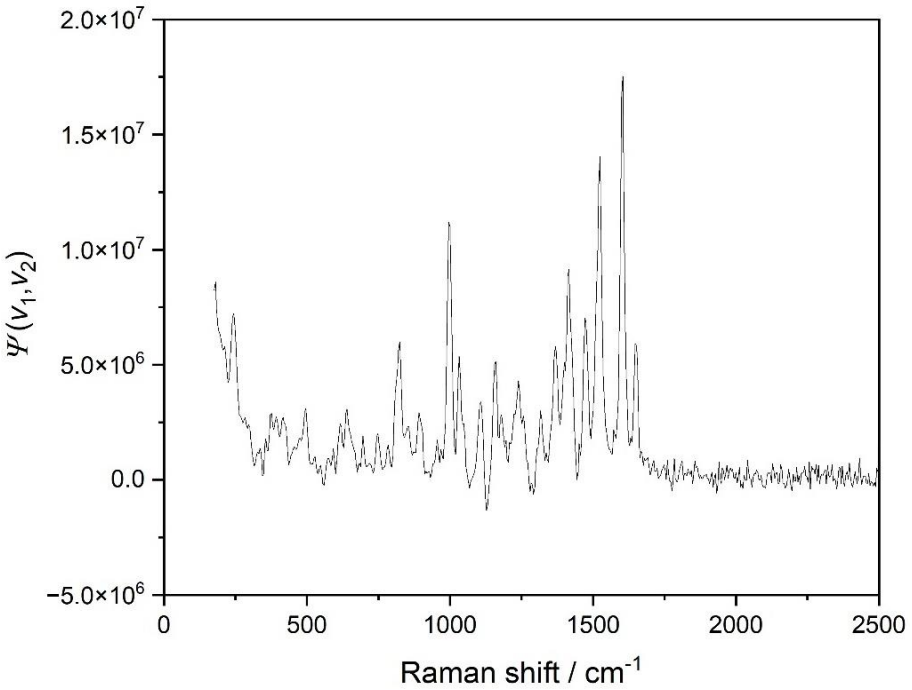

Fig. 6. A slice through the full 2T2D correlation Raman spectra at ν_1 = 1444 cm^{-1} (see text for details)

Complementary conclusions were derived from the analysis of the 2T2D correlation maps generated from the XRD patterns. As evident from Figure 4, a series of distinct, high-intensity, and clearly distinguishable peaks were observed in the asynchronous 2T2D correlation map.

Figure 7 shows a slice through the full asynchronous 2T2D correlation map computed from powder XRD data taken at $(2\theta)_1 = 9.00^o$. A series of positive intensity peaks ($\Psi((2\theta)_1, (2\theta)_2) > 0$) were observed, with the most prominent ones being positioned at $(2\theta)_2$ = 6.14, 9.14, 9.48, 10.24, 10.55, 11.84, 12.17, 17.04, 19.43, 21.57, 22.67, 23.30, 23.68, and 24.36º. Comparison with available literature data strongly implied that the observed sequence of signals correspond to reflections arising from polymorph X of atorvastatin calcium trihydrate. The positive sign of the asynchronous peaks ($\Psi((2\theta)_1, (2\theta)_2) > 0$), by contrast, indicated that the contribution of the species giving rise to the signal at $(2\theta)_1 = 9^o$ (phase I of the investigated compound) was dominantly represented in $s(2\theta)$ relative to $r(2\theta)$. Analogous conclusions were drawn from the slice through the full asynchronous 2T2D correlation map computed from powder XRD data collected at $(2\theta)_1 = 21.40^o$ (Fig. 8). We note, however, that polymorph X is present only in trace amounts.

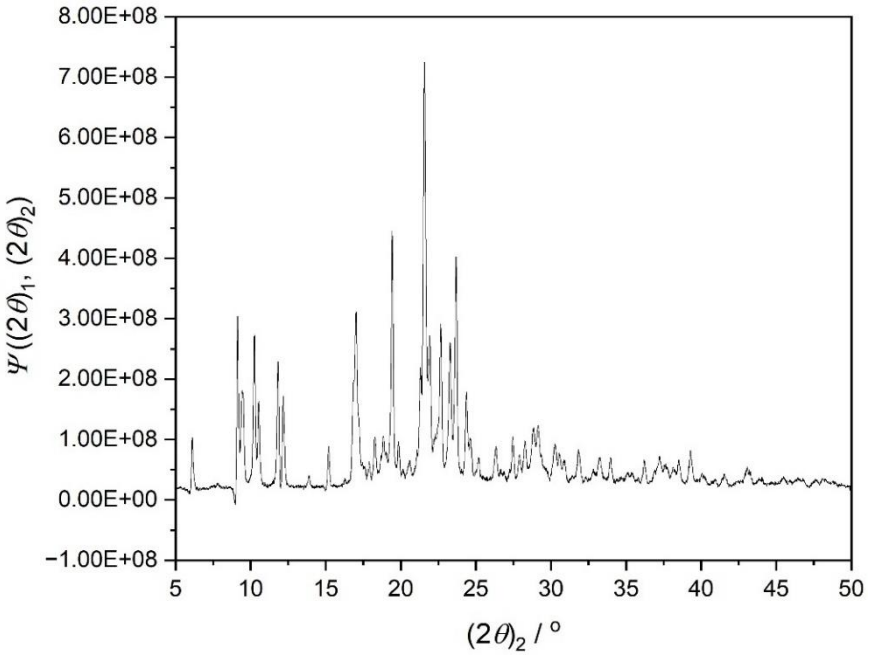

Fig. 7. A slice through the full asynchronous 2T2D correlation map computed from powder XRD data collected at $(2\theta)_1 = 9.00^o$.

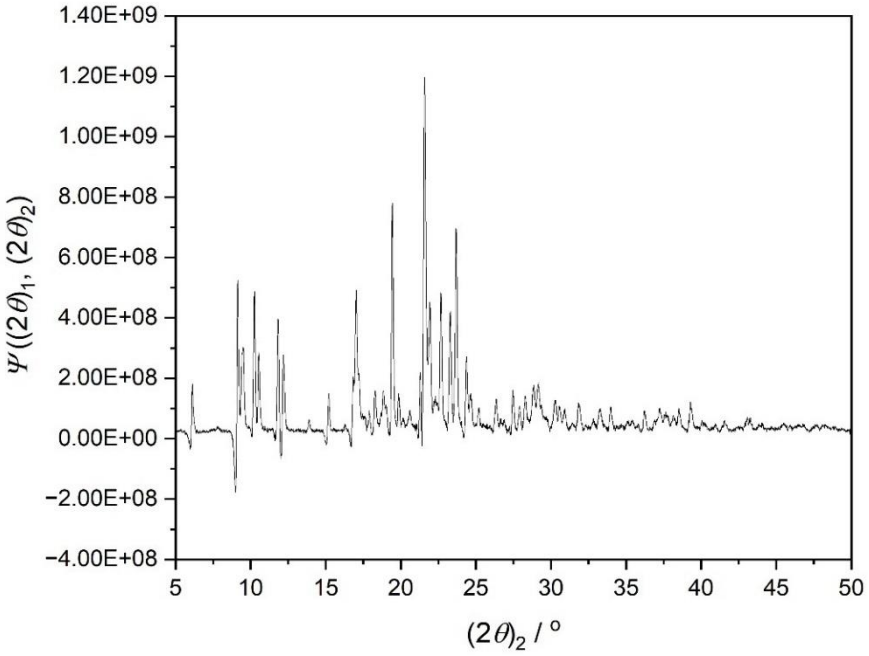

Fig. 8. A slice through the full asynchronous 2T2D correlation map computed from powder XRD data collected at $(2\theta)_1 = 21.40^o$

4. CONCLUSIONS

In this work, two-trace two-dimensional correlation analysis of Raman spectra and X-ray diffraction patterns was implemented to provide discriminant analysis of atorvastatin calcium trihydrate raw materials from two different manufacturers. Single-parameter trace similarity measures, such as the cosine similarity score and Pearson's correlation coefficient, while useful in the context of similarity analysis within sets containing multiple samples, failed to capture the differences (or lack thereof) between complex two-dimensional traces that contain a wide variety of signals. In contrast, the discriminant potential of the asynchronous 2T2D correlation maps, computed from the Raman spectral traces and XRD patterns, for resolving spectral bands originating from multiple species proved exceptional. These two types of 2T2D correlation maps provided complementary insights into the phase composition of the investigated samples. Detailed analysis of the 2T2D correlation spectra enabled potential identification of different atorvastatin calcium phases as well as their degradation products.

5. REFERENCES

(1) Jacobson, T. A.; Ito, M. K.; Maki, K. C.; Orringer, C. E.; Bays, H. E.; Jones, P. H.; McKenney, J. M.; Grundy, S. M.; Gill, E. A.; Wild, R. A.; Wilson, D. P.; Brown, W. V. National lipid association recommendations for patient-centered management of dyslipidemia: part 1--full report. *J. Clin. Lipidol.* **2015**, *9*, 129–169.

(2) Jacobson, T. A.; Maki, K. C.; Orringer, C. E.; Jones, P. H.; Kris-Etherton, P.; Sikand, G.; La Forge, R.; Daniels, S. R.; Wilson, D. P.; Morris, P. B.; Wild, R. A.; Grundy, S. M.; Daviglus, M.; Ferdinand, K. C.; Vijayaraghavan, K.; Deedwania, P. C.; Aberg, J. A.; Liao, K. P.; McKenney, J. M.; Ross, J. L.; Braun, L. T.; Ito, M. K.; Bays, H. E.; Brown, W. V.; Underberg, J. A.; NLA Expert Panel. National Lipid Association Recommendations for Patient-Centered Management of Dyslipidemia: Part 2. *J. Clin. Lipidol.* **2015**, *9*, S1–S122.

(3) Burger, P. M.; Dorresteijn, J. A. N.; Koudstaal, S.; Holtrop, J.; Kastelein, J. J. P.; Jukema, J. W.; Ridker, P. M.; Mosterd, A.; Visseren, F. L. J. Course of the effects of LDL-cholesterol reduction on cardiovascular risk over time: A meta-analysis of 60 randomized controlled trials. *Atherosclerosis* **2024**, *396*, 118540.

(4) Zubiaur, P.; Benedicto, M. D.; Villapalos-García, G.; Navares-Gómez, M.; Mejía-Abril, G.; Román, M.; Martín-Vílchez, S.; Ochoa, D.; Abad-Santos, F. SLCO1B1 Phenotype and CYP3A5 Polymorphism Significantly Affect Atorvastatin Bioavailability. *J. Pers. Med.* **2021**, *13*, 11.

(5) Salazar-Barrantes, K. A.; Abdala-Saiz, A.; Vega-Baudrit, J. R.; Navarro-Hoyos, M.; Araya-Sibaja, A. M. Formulation and evaluation of atorvastatin calcium trihydrate Form I tablets. *PLoS ONE* **2025**, *20*, e0317407.

(6) Trkmen, D.; Liang, X.; Masoli, J. A. H.; Gill, D.; Pilling, L. C.; Bowden, J.; Understanding the causes and consequences of low statin adherence: evidence from UK Biobank primary care data. *BMC Medicine* **2025**, *23*, 436.

(7) Sever, P. S. Supplemental material - Long-term benefits of atorvastatin on the incidence of cardiovascular events: the ASCOT-Legacy 20-year follow-up. **2025**, *111*, 769–775.

(8) Byrn, S. R.; Pfeiffer, R.; Ganey, M.; Hoiberg, C.; Poochikian, G.; Crystalline R-(+)-2-(4-fluorophenyl)-β,δ-dihydroxy-5-(1-methylethyl)-3-phenyl-4-phenylaminocarbonyl-1H-pyrrole-1-heptanoic acid hemi calcium salt (atorvastatin). In: Polymorphism in Pharmaceutical Solids (Brittain HG, Ed.), Marcel Dekker, 2007.

(9) Kogawa, A. C.; Pires, A. E. D. T.; Salgado, H. R. N.; Atorvastatin: A review of analytical methods for pharmaceutical quality control and monitoring. *Journal of AOAC International* **2019**, *102*, 801–811.

(10) Agrawal, K.; Idhate, A.; Haswani, N.; Jain, P.; Kalaskar, M.; Analytical techniques for monitoring atorvastatin in pharmaceuticals: a detailed review. *Int. J. Pharm. Sci.* **2025**, 3, 2894–2917.

(11) Lennernas, H. Clinical pharmacokinetics of atorvastatin. *Clin. Pharmacokinet.* **2003**, *42*, 1141–1160.

(12) Sonje, V. M.; Kumar, M. L.; Kohli, C. L.; Puri, G.; Jain, V.; Atorvastatin Calcium. In: Profiles of Drug Substances, Excipients and Related Methodology, 2010, Elsevier, pp. 1–70.

(13) Wasserman, L. All of statistics, Springer, 2004.

(14) Samuel, A. Z.; Mukojima, R.; Horii, S.; Ando, M.; Egashira, S.; Nakashima, T.; Iwatsuki, M.; Takeyama, H. On selecting a suitable spectral matching method for automated analytical applications of Raman spectroscopy. *ACS Omega* **2021**, *6*, 2060-2065.

(15) Lepine, M. College statistics. St. Clair College AA&T, 2022.

(16) Noda, I. Two-trace two-dimensional (2T2D) correlation spectroscopy – A method for extracting useful information from a pair of spectra. *J. Mol. Struct.* **2018**, *1160*, 471–478.

(17) Noda, I. Two-trace two-dimensional (2T2D) correlation applied to a number of spectra beyond a simple pair. *Spectrochim. Acta A: Mol. Biomol. Spectrosc.* **2022**, *277*, 121258.

(18) Jeonga, S.; Chunga, H.; Combining two-trace two-dimensional correlation analysis and convolutional autoencoder-based feature extraction from an entire correlation map to enhance the accuracy of vibrational spectroscopic discriminant analysis, SSRN, 2024.

(19) Noda, I. Frontiers of two-dimensional correlation spectroscopy. Part 2. Perturbation methods, fields of applications, and types of analytical probes. *J. Mol. Struct.* **2014**, *1069*, 23.

(20) Noda, I. Closer examination of two-trace two-dimensional (2T2D) correlation spectroscopy. *J. Mol. Struct.* **2020**, *1213*, 128194.

(21) Mayerhöfer, T. G.; Noda, I.; Popp, J. Dispersion Analysis of Perpendicular Modes Using a Hybrid Two-Trace Two-Dimensional (2T2D) Smart Error Sum. *Appl. Spectrosc.* **2025**, *79*, 1.

(22) Noda, I. Techniques useful in two-dimensional correlation and codistribution spectroscopy (2DCOS and 2DCDS) analyses. *J. Mol. Struct.* **2016**, *1124*, 29.

(23) Sohng, W.; Eum, C.; Chung, H.; Exploring two-trace two-dimensional (2T2D) correlation spectroscopy as an effective approach to improve accuracy of discriminant analysis by highlighting asynchronous features in two separate spectra of a sample. *Anal. Chim. Acta* **2021**, *1152*, 338255.

(24) Salazar-Barrantes, K. A.; Vega-Baudrit, J. R.; Navarro-Hoyos, M.; Araya-Sibaja, A. M. Thermoanalytical techniques applied to the solid-state characterization of atorvastatin calcium trihydrate form I. *Chem. Thermodyn. Therm. Anal.* **2024**, *14*, 100130.

(25) Oprica, M.; Iota, M.; Daescu, M.; Fejer, S. N.; Negrila, C.; Baibarac, M. Spectroscopic studies on photodegradation of atorvastatin calcium. *Sci. Rep.* **2021**, *11*, 15338.

(26) Skorda, D.; Kontoyannis, C. G. Identification and quantitative determination of atorvastatin calcium polymorph in tablets using FT-Raman spectroscopy. *Talanta* **2008**, *74*, 1066–1070.